The Plant Cell, Vol. 27: 2042–2056, July 2015, www.plantcell.org

Phosphorylation of the Plant Immune Regulator RPM1-INTERACTING PROTEIN4 Enhances Plant Plasma Membrane H+-ATPase Activity and Inhibits Flagellin-Triggered Immune Responses in Arabidopsis[OPEN]

DongHyuk Lee,[a] Gildas Bourdais,[b] Gang Yu,[a] Silke Robatzek,[b] and Gitta Coaker[a,1]

[a] Department of Plant Pathology, University of California, Davis, California 95616
[b] The Sainsbury Laboratory, Norwich NR4 7UH, United Kingdom

ORCID ID: 0000-0003-0899-2449 (G.C.)

The *Pseudomonas syringae* effector AvrB targets multiple host proteins during infection, including the plant immune regulator RPM1-INTERACTING PROTEIN4 (RIN4) and RPM1-INDUCED PROTEIN KINASE (RIPK). In the presence of AvrB, RIPK phosphorylates RIN4 at Thr-21, Ser-160, and Thr-166, leading to activation of the immune receptor RPM1. Here, we investigated the role of RIN4 phosphorylation in susceptible *Arabidopsis thaliana* genotypes. Using circular dichroism spectroscopy, we show that RIN4 is a disordered protein and phosphorylation affects protein flexibility. RIN4 T21D/S160D/T166D phosphomimetic mutants exhibited enhanced disease susceptibility upon surface inoculation with *P. syringae*, wider stomatal apertures, and enhanced plasma membrane H+-ATPase activity. The plasma membrane H+-ATPase AHA1 is highly expressed in guard cells, and its activation can induce stomatal opening. The *ripk* knockout also exhibited a strong defect in pathogen-induced stomatal opening. The basal level of RIN4 Thr-166 phosphorylation decreased in response to immune perception of bacterial flagellin. RIN4 Thr166D lines exhibited reduced flagellin-triggered immune responses. Flagellin perception did not lower RIN4 Thr-166 phosphorylation in the presence of strong ectopic expression of AvrB. Taken together, these results indicate that the AvrB effector targets RIN4 in order to enhance pathogen entry on the leaf surface as well as dampen responses to conserved microbial features.

INTRODUCTION

Plant cells have the ability to recognize pathogen-derived molecules or proteins and mount a successful defense response through their innate immune system (Spoel and Dong, 2012). Germ-line-encoded plant immune receptors, often with extracellular domains, recognize conserved microbe-associated molecular patterns (MAMPs or PAMPs) and activate pattern-triggered immunity (PTI) (Spoel and Dong, 2012). Activation of PTI leads to effective defense responses, including mitogen-activated protein kinase (MAPK) and calcium-dependent protein kinase signaling, leading to transcriptional reprogramming, production of extracellular reactive oxygen species (ROS), and cell wall fortification in the form of callose deposition (Henry et al., 2013). Activation of PTI is thought to inhibit most potential pathogens, but specialized pathogens can deliver apoplastic or intracellular effectors to disable PTI in susceptible plant genotypes. The second layer of the plant immune system relies primarily on intracellular receptors recognizing pathogen effectors delivered into host cells during infection, resulting in effector-triggered immunity (ETI). Most plant ETI receptors possess central nucleotide binding and C-terminal leucine-rich repeat (NLR) domains. Recent research has highlighted differences in perception and localization across NLRs. Certain NLRs require dynamic nuclear relocalization for function (Slootweg et al., 2010), some function outside of the nucleus (Gao et al., 2011), some function as pairs to recognize diverse pathogens (Narusaka et al., 2009), and some require downstream "helper" NLRs for full immunity (Bonardi et al., 2011). Despite these differences, there are commonalities in classical ETI-related phenotypes. Common cellular changes during ETI also include sustained ROS production, Ca^{2+} signaling, transcriptional reprogramming of the host cell toward defense, and a form of programmed cell death at the site of infection, called the hypersensitive response (Henry et al., 2013).

The bacterial pathogen *Pseudomonas syringae* pv *tomato* (*Pto*) and the interaction with its hosts tomato (*Solanum lycopersicum*) and *Arabidopsis thaliana* have been intensely studied, and this has significantly enhanced our understanding of plant immunity and microbial pathogenesis (Xin and He, 2013). Plant pathogenic bacteria can deliver 20 to 40 effector proteins into host cells using the type III secretion system. *Pto* strain DC3000 delivers ~28 effectors into host cells during infection, many of which are capable of suppressing PTI (Lindeberg et al., 2012). Despite the number of different pathogen effectors from diverse microorganisms, large-scale analyses of effector targets have revealed that effectors do not randomly target host proteins, but rather converge upon a limited set of host targets representing key nodes in immune signaling (Mukhtar et al., 2011). For

[1] Address correspondence to glcoaker@ucdavis.edu.
The author responsible for distribution of materials integral to the findings presented in this article in accordance with the policy described in the Instructions for Authors (www.plantcell.org) is: Gitta Coaker (glcoaker@ucdavis.edu).
[OPEN] Articles can be viewed online without a subscription.
www.plantcell.org/cgi/doi/10.1105/tpc.114.132308

example, multiple effectors target PTI receptors, downstream MAPKs, and vesicle trafficking of antimicrobial compounds to the point of pathogen attack (Lindeberg et al., 2012).

The Arabidopsis protein RIN4 (RPM1-INTERACTING PROTEIN4) is targeted by multiple bacterial effectors, including HopF2, AvrPto, AvrRpt2, AvrB, and AvrRpm1 (Mackey et al., 2002, 2003; Axtell and Staskawicz, 2003; Luo et al., 2009; Wilton et al., 2010). RIN4 is widely conserved across land plants and has been demonstrated to be an important regulator of NLR signaling in Arabidopsis, tomato, soybean (*Glycine max*), and lettuce (*Lactuca sativa*) (Axtell and Staskawicz, 2003; Mackey et al., 2003; Jeuken et al., 2009; Luo et al., 2009; Selote and Kachroo, 2010). RIN4 is a key accessory protein that associates with the plasma membrane localized NLRs, RPM1 (RESISTANCE TO PSEUDOMONAS SYRINGAE PV MACULICOLA1), and RPS2 (RESISTANCE TO PSEUDOMONAS SYRINGAE PV TOMATO2) (Mackey et al., 2002, 2003; Axtell and Staskawicz, 2003). The RPS2 immune receptor recognizes the absence of RIN4 induced by the *Pto* effector AvrRpt2, a protease (Axtell and Staskawicz, 2003; Mackey et al., 2003). Therefore, the *rin4* knockout (KO) is only viable in the *rps2-101c* mutant background (Axtell and Staskawicz, 2003). The RPM1 immune receptor recognizes the presence of the *P. syringae* effectors AvrB and AvrRpm1 (Mackey et al., 2002). Although both effectors induce RIN4 phosphorylation in planta, they are unable to directly phosphorylate RIN4. RPM1-INDUCED PROTEIN KINASE (RIPK), a receptor-like cytoplasmic kinase, phosphorylates RIN4 at three residues: Thr-21, Ser-160, and Thr-166 (Liu et al., 2011). RIN4 phosphorylation mimics exhibit constitutive activation of RPM1-mediated defense responses, Thr-166 phosphorylation is induced by AvrB/AvrRpm1, and RIN4 Thr-166 phosphorylation mimics are sufficient to activate RPM1 in the absence of pathogen effectors (Chung et al., 2011; Liu et al., 2011). Recently, the cyclophilin ROC1 has been demonstrated to isomerize RIN4 Pro-149 and has been implicated in the activation of RPM1 (Li et al., 2014b). RIN4 Thr-166 phosphorylation inhibits the ROC1-RIN4 association, and RIN4 ΔP149 is also sufficient to activate RPM1-mediated responses (Li et al., 2014b).

The Arabidopsis *rin4* knockout also exhibits enhanced PTI responses, with lower bacterial growth after spray inoculation and enhanced callose deposition upon flagellin treatment (Kim et al., 2005). The AvrB and AvrRpm1 effectors, which induce RIN4 phosphorylation, suppress multiple PTI based responses in susceptible genotypes (Kim et al., 2005; Chung et al., 2014). Recently, Chung et al. (2014) found that mimicking RIN4 Thr-166 phosphorylation suppressed PTI responses. RIN4 can be phosphorylated at multiple residues, including Ser-141, whose phosphorylation is induced during flagellin perception, enhances PTI responses, and is epistatic to Thr-166 phosphorylation (Nühse et al., 2007; Chung et al., 2014). Collectively, these experiments indicate that RIN4 is differentially phosphorylated, with distinct residues playing important roles in defense activation or suppression depending on the Arabidopsis genotype.

In addition to RIPK and the NLRs RPM1 and RPS2, purification of native RIN4 complexes has identified additional RIN4 associated proteins (Liu et al., 2009a, 2009b, 2011). RIN4 can directly interact with the C-terminal regulatory domain of AHA1 and AHA2, two closely related plasma membrane H^+-ATPases, and acts as a positive regulator of the proton pump. AHA activation initiates an electrochemical gradient driving the import of charged solutes, leading to water import and stomatal opening (Elmore and Coaker, 2011). Guard cells are active immune signaling cells and rapidly close upon sensing microbial patterns, such as bacterial flagellin, effectively blocking pathogen entry into the leaf interior (Melotto et al., 2006). Virulent pathogens are able to initiate stomatal reopening through a variety of different mechanisms (Elmore and Coaker, 2011). *Pto* uses coronatine, a jasmonic acid (JA) mimic, to induce stomatal opening (Melotto et al., 2006). The *Pto* effector HopM1 can also suppress stomatal immunity (Lozano-Durán et al., 2014). RIN4, AHA1/2, and multiple innate immune receptors are expressed in guard cells (Ueno et al., 2005; Liu et al., 2009b). The *rin4* knockout line exhibits reduced PM H^+-ATPase activity and its stomata cannot be reopened by virulent *P. syringae* (Liu et al., 2009b).

In this study, we focus on the role of RIN4 phosphorylation in susceptible Arabidopsis genotypes. We demonstrate that RIN4 phosphorylation mimics exhibit enhanced flexibility, can interact more strongly with AHA1, enhance AHA activity, and exhibit wider basal stomatal apertures. The basal level of RIN4 Thr-166 phosphorylation decreases during PTI, and phosphorylation mimics exhibit reduced flagellin-triggered immune responses. Thus, RIN4 phosphorylation acts to promote *P. syringae* virulence in susceptible plant genotypes.

RESULTS

RIN4 Is an Intrinsically Disordered Protein

Despite the conservation of RIN4 in land plants and its importance in regulating plant innate immunity, RIN4 has no similarity to known enzymes and its specific biochemical function remains unknown. In order to gain insight into the predicted structure of RIN4, in silico predictions of secondary structure were determined. Using the Protein Disorder Prediction System (PrDOS) server, RIN4 was predicted to exhibit a high level of intrinsic disorder (Figures 1A and 1B) (Ishida and Kinoshita, 2007). Intrinsically disordered regions or proteins are flexible segments lacking secondary or tertiary structure (Dyson and Wright, 2005). Proteins exhibiting high levels of intrinsic disorder can transition to a more folded state upon client binding and can associate with multiple protein clients with both high specificity and low affinity (Dyson and Wright, 2005). The regions of RIN4 that are predicted to be ordered flank RIPK phosphorylation sites, sites targeted by effectors, and also include the C-terminal membrane targeting region (amino acids 14 to 28, 147 to 174, and 201 to 209), highlighting the importance of phosphorylation for RIN4 function (Figures 1A and 1B). In order to validate the intrinsic disorder prediction, recombinant His6-RIN4 was purified from *Escherichia coli* and subjected to circular dichroism (CD) spectroscopy (Figure 1C). Consistent with the in silico prediction, full-length RIN4 circular dichroism spectra displayed a characteristic shape, including low ellipticity at 190 nm and strong negative ellipticity at 200 nm, consistent with an intrinsically disordered protein (Figure 1E).

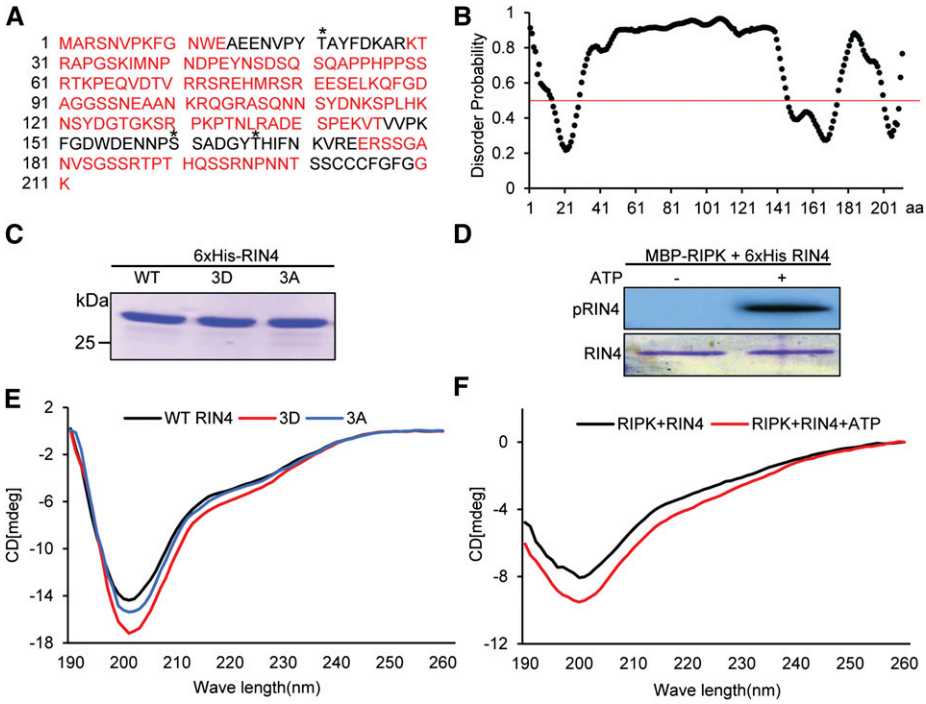

Figure 1. RIN4 Is an Intrinsically Disordered Protein, and Phosphorylation Affects Flexibility.

(A) PrDOS prediction of disorder in RIN4. Red and black amino acid sequences indicate predicted disordered and ordered regions, respectively. Asterisks indicate phosphorylated residues on RIN4 by RIPK (Thr-21, Ser-160 and Thr-166).

(B) PrDOS plot of disorder probability of each residue along the sequence of RIN4. Residues above the red threshold line in this plot are predicted to be disordered.

(C) SDS-PAGE gel stained with Coomassie blue demonstrating the purity of recombinant wild-type RIN4 (WT RIN4), phosphorylation mimic (RIN4 3D), or phosphorylation null (RIN4 3A). The residues Thr-21, Ser-160, and Thr-166 were mutated to D or A in the RIN4 phosphorylation mimic and phosphorylation null, respectively.

(D) In vitro phosphorylation of RIN4 by RIPK. Recombinant RIPK (MBP-RIPK) was incubated with recombinant wild type RIN4 (WT RIN4) in the presence and absence of ATP. RIPK was subsequently removed based on its molecular mass using a centrifugal filter unit. Top panel: RIN4 pThr166 (pRIN4) proteins detected by anti-pRIN4 Thr-166 antibody. Bottom panel: SDS-PAGE gel stained with Coomassie blue confirmed equal amounts of RIN4.

(E) Far-UV CD spectroscopy of purified RIN4 proteins from **(C)**. Wild-type RIN4's trace is shown in black, the RIN4 phosphorylation mimic (3D) trace is shown in red, and the RIN4 phosphorylation null (3A) trace is shown in blue.

(F) Far-UV CD spectroscopy of phosphorylated RIN4 proteins from **(D)**. Unphosphorylated RIN4's trace is shown in black and phosphorylated RIN4's trace is shown in red.

Mimicking RIN4 phosphorylation by substituting the phosphorylated threonine (T) residue 166 to glutamatic (E) or aspartic acid (D) is sufficient to activate RPM1-triggered immunity in planta (Chung et al., 2011; Liu et al., 2011). These data indicate that phosphorylated RIN4 and phosphorylation mimics impart similar folds. To investigate the role of RIN4 phosphorylation in changing secondary structure, RIN4 T21/S160/T166 residues were substituted with aspartic acid (D) to generate a RIN4 phosphorylation mimic (RIN4 3D). Recombinant His6-RIN4 3D was purified from *E. coli* and subjected to CD spectroscopy (Figure 1C). Interestingly, RIN4 3D CD spectra exhibited a shifted shape and stronger magnitude around 200 nm compared with wild-type RIN4 (Figure 1E). A stronger magnitude at 200 nm is indicative of a more flexible structure (Greenfield, 2006). To determine if phosphorylated RIN4 residues are generally important for protein flexibility, we mutated all three residues to alanine (A) to generate a RIN4 dephosphorylation mimic (RIN4 3A). Recombinant His6-RIN4 3A protein exhibited a slightly stronger magnitude than wild type RIN4, but not to the same extent as RIN4 3D (Figures 1C and 1E). Next, the importance of individual residues was examined for altering RIN4 secondary structure using CD spectroscopy (Supplemental Figure 1). The RIN4 T21D mutant displayed a similar CD spectra compared with RIN4 3D protein, while the RIN4 T166D mutant displayed decreased magnitude at 200 nm (Supplemental Figure 1). These data indicate that the RIN3 3D phosphorylation mimic is more flexible than wild-type RIN4 and the primary residue contributing to increased flexibility is Thr-21.

To determine the general secondary structure of phosphorylated RIN4, RIN4 was phosphorylated in vitro in the presence of the RIPK kinase (Supplemental Figure 2). As a negative control, RIN4 was incubated with RIPK in the absence of ATP. RIPK was subsequently removed from the sample based on its molecular mass using a centrifugal filter unit (Supplemental Figure 2). Protein gel blotting with antibody recognizing RIN4 pThr166 confirmed RIN4 phosphorylation in the presence of RIPK and

ATP (Figure 1D). The samples were subsequently subjected to CD spectroscopy and phosphorylated RIN4 exhibited a shifted shape and stronger magnitude around 200 nm compared with unphosphorylated RIN4 (Figure 1F). Therefore, these data demonstrate that phosphorylated RIN4 as well as the 3D phosphorylation mimic are more flexible than wild-type RIN4, and phosphorylation can affect RIN4 folding.

Gel filtration chromatography was used to determine the mobility of RIN4 and RIN4 phosphorylation mutants. Wild-type recombinant RIN4, RIN4 3D, and RIN4 3A exhibited similar elution profiles (Supplemental Figure 3). The major elution peak corresponded to a 55-kD globular protein. The only visible protein in the major peak was full-length His6-RIN4, which is predicted to have a molecular mass of 26 kD (Supplemental Figure 3D). The elution from the gel filtration column is consistent with either dimerization or an extended conformation due to intrinsic disorder. All three proteins exhibited a minor elution peak corresponding to a 13-kD globular protein (Supplemental Figure 3). The visible proteins in the minor peaks included a small amount of full-length RIN4 and a higher amount of cleaved or partially degraded RIN4 (Supplemental Figure 3D). The RIN4 3A sample possessed a smaller minor peak and smaller amount of cleaved RIN4. Thus, it is possible that the 3A mutation affects protein stability in vitro. Collectively, these data indicate that mutating phosphorylated RIN4 residues does not grossly affect protein folding.

RIN4 Phosphorylation Mimics Exhibit Enhanced Disease Susceptibility in the Absence of RPM1 and RPS2 and Can Interact More Strongly with AHA1

The Arabidopsis Col-0 genome encodes 149 NLRs, but the NLR complement can vary significantly across Arabidopsis ecotypes and land plants (Meyers et al., 2003; McDowell and Simon, 2006). The AvrB effector was originally cloned from *P. syringae* pv *glycinea*, the causal agent of bacterial blight of soybean (Tamaki et al., 1988). AvrB has been identified in other *P. syringae* pathovars and can infect plant genotypes lacking corresponding NLRs. *Pto* DC3000 expressing empty vector or the AvrB effector was used to syringe infiltrate *rpm1/rps2* lines, followed by protein gel blotting with antisera recognizing RIN4 and phosphorylated RIN4 Thr-166 (anti-pRIN4). At 5 and 10 h postinfiltration, RIN4 pThr166 was induced in the presence of AvrB (Supplemental Figure 4). Therefore, RIN4 phosphorylation is induced in the presence of AvrB in the absence of the RPM1 and RPS2 immune receptors.

In order to investigate the role of bacterial-induced RIN4 phosphorylation in susceptible plant genotypes lacking the RPM1 and RPS2 immune receptors, we complemented the *rpm1 rps2 rin4* triple mutant with T7-tagged genomic *RIN4* under the control of its native promoter (*T7-RIN4*), the RIN4 phosphomimetic mutant where Thr-21/Ser-160/Thr-166 residues were mutated to Asp (*T7-RIN4 3D*), or the phospho-null mutant where Thr-21/Ser-160/Thr-166 residues were mutated to Ala (*T7-RIN4 3A*). Homozygous T3 transgenic lines were carefully expression matched for equal RIN4 expression compared with *rpm1/rps2* by protein gel blot (Figure 2A). Due to the addition of the T7 epitope tag, the size of RIN4 in the transgenic lines is slightly larger than wild-type RIN4 present in *rpm1/rps2* (Figure 2A). In order to verify that *T7-RIN4* can complement the *rin4* KO, plants were spray inoculated with virulent *Pto* DC3000 and bacterial growth was enumerated 4 d postinoculation (Figure 2B). Genetically, *RIN4* acts as a negative regulator of basal defense (Kim et al., 2005). As expected, *rpm1/rps2/rin4* exhibited reduced bacterial growth compared with *rpm1/rps2*, and this decrease in bacterial growth could be complemented by two independent transgenic lines expressing *T7-RIN4* (Figure 2B). Transgenic *T7-RIN4 3D* and *T7-RIN4 3A* lines were spray inoculated with virulent *Pto* DC3000 and bacterial growth was enumerated 4 d postinoculation (Figure 2C). *T7-RIN4 3D* lines exhibited significantly higher bacterial growth (5-fold) compared with wild-type *T7-RIN4* and *T7-RIN4 3A* dephosphorylation mimics (Figure 2C). Thus, mimicking RIN4 phosphorylation at Thr-21/Ser-160/Thr-166 significantly promotes bacterial virulence in susceptible plant genotypes.

The *rin4* KO exhibits reduced AHA activity, and addition of recombinant RIN4 protein to plasma membranes extracted from the *rpm1/rps2/rin4* genotype can enhance AHA activity in this semi in vitro assay (Liu et al., 2009b). In order to determine the role of RIN4 phosphorylation for promoting AHA activity, inside-out plasma membrane vesicles were purified from *rpm1/rps2/rin4*, and H^+ transport was measured in the presence and absence of recombinant RIN4. Interestingly, addition of purified His6-RIN4 3D recombinant protein enhanced AHA activity significantly more than addition of wild-type His6-RIN4 (Figures 3A and 3B). Purified recombinant His6-RIN4 3A protein was also analyzed for its ability to enhance AHA activity. Although the addition of His6-RIN4 3A recombinant protein did not significantly enhance AHA activity, we observed a consistent trend where 3A protein led to an intermediate level of AHA activation between that of the wild type and 3D (Figure 3C). Single T21D, S160D, and T166D phosphomimetic proteins were unable to enhance AHA activity beyond that observed from wild-type RIN4 (Figure 3C).

Previously, RIN4 was demonstrated to interact with the C-terminal regulatory domain of AHA1/2 plasma membrane H^+-ATPases (Liu et al., 2009b). The association between AHA1 and RIN4 was examined using a split luciferase assay after transient expression of AHA1-NLuc and CLuc-RIN4 in *Nicotiana benthamiana.* After the addition of luciferin, positive signals were imaged using a CCD camera and quantified on a luminometer (Figure 4). As expected, wild-type CLuc-RIN4 associated with AHA1-NLuc (Figure 4). Consistent with the enhancement of enzymatic activity, CLuc-RIN4 3D exhibited a significantly stronger association with AHA1-NLuc compared with wild-type RIN4 or single RIN4 phosphorylation mimics (Figures 4A and 4B). RIN4 3A exhibited an intermediate phenotype (Figure 4A). All RIN4 proteins were expressed by protein gel blotting (Figures 4C and 4D). Taken together, these results indicate that modification of all three residues is necessary for enhancing AHA activity beyond the effect of wild-type RIN4.

RIN4 Phosphorylation Mimics Exhibit Wider Basal Stomatal Apertures and the *ripk* Knockout Is Insensitive to Coronatine-Induced Stomatal Opening

Because of the enhanced disease susceptibility phenotype after surface inoculation with *Pto* DC3000 in *T7-RIN4 3D* (Figure 2), we examined the role of RIPK and RIN4 phosphorylation mimics

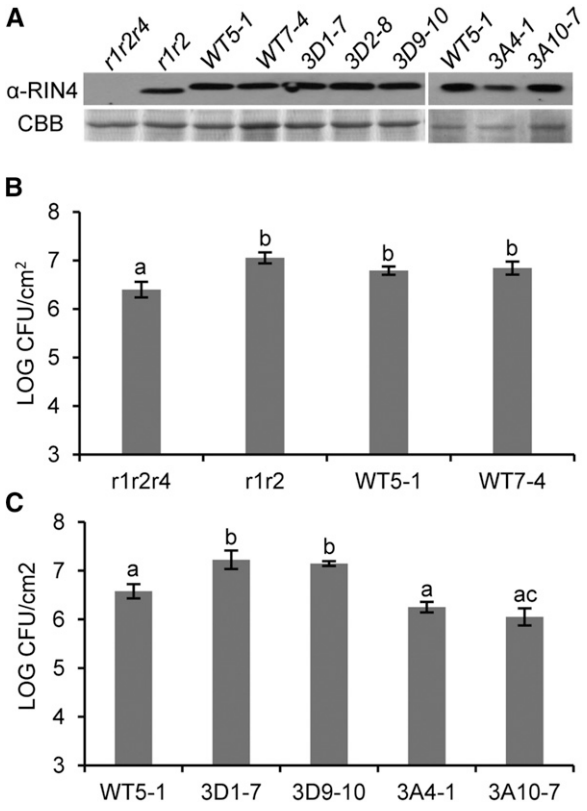

Figure 2. Transgenic Lines Expressing the RIN4 Phosphorylation Mimic Exhibit Enhanced Disease Susceptibility to *P. syringae* DC3000 in a Susceptible Genetic Background.

The Arabidopsis *rpm1/rps2/rin4* mutant was complemented with T7-tagged with genomic *RIN4* (WT), *gRIN4 3D* (3D), or *gRIN4 3A* (3A) under the control of *RIN4*'s native promoter. RIN4 Thr-21/Ser-160/Thr-166 residues are mutated to D or A in 3D or 3A lines, respectively.

(A) Anti-RIN4 protein gel blot illustrating RIN4 expression in T4 homozygous lines expressing wild type (WT 5-1 and WT 7-4), phosphorylation mimics (3D 1-7, 3D 2-8, and 3D 9-10), and phosphor-null mutants (3A 4-1 and 3A 10-7) in the *rpm1/rps2/rin4* genetic background. Total proteins were extracted from 10-d-old seedlings and subjected to immunoblot with anti-RIN4. SDS-PAGE gel stained with Coomassie blue (CBB) was used as a loading control. *r1r2r4* = *rpm1/rps2/rin4*; *r1r2* =*rpm1/rps2*. The white line indicates that samples were run on two separate protein gel blots but extracted and processed at the same time.

(B) Complementation analysis with *npro:T7*-gRIN4 in the *rpm1/rps2/rin4* mutant. Four-week-old *r1r2*, *r1r2r4*, or wild-type RIN4 complementation lines (WT RIN4 5-1 and 7-4) were spray-inoculated with 1×10^8 cfu/mL of *Pto* DC3000. Bacterial population sizes were quantified 4 d post-inoculation. Results represent means ± SE, $n = 6$.

(C) RIN4 phosphorylation mimic lines (RIN4 3D) exhibit enhanced disease susceptibility to *Pto* DC3000. Wild-type RIN4 (WT 5-1), RIN4 phosphorylation mimic (3D 1-7 and 9-10), or phosphor-null (3A 4-1 and 10-7) lines were inoculated and bacterial growth was determined as described in **(B)**. Results represent means ± SE, $n = 6$. Different letters above bars indicate statistical differences in means, detected by a Fisher's LSD ($\alpha = 0.05$).

in altering MAMP-induced stomatal closure and coronatine-induced stomatal opening. Confocal laser scanning microscopy was employed to measure stomatal apertures of individual KO lines and transgenic seedlings. In order to assess MAMP-induced stomatal closure, 2-week-old seedlings were treated with 10 μM flg22 (a 22-amino acid epitope of bacterial flagellin). To assess coronatine-induced stomatal opening, seedlings were co-incubated with 10 μM flg22 and 300 ng/mL coronatine for 2 h prior to imaging. The *ripk* KO possessed a strong defect in coronatine-induced stomatal opening in either the Landsberg *erecta* or Col-0 background (Figure 5A; Supplemental Figure 5).

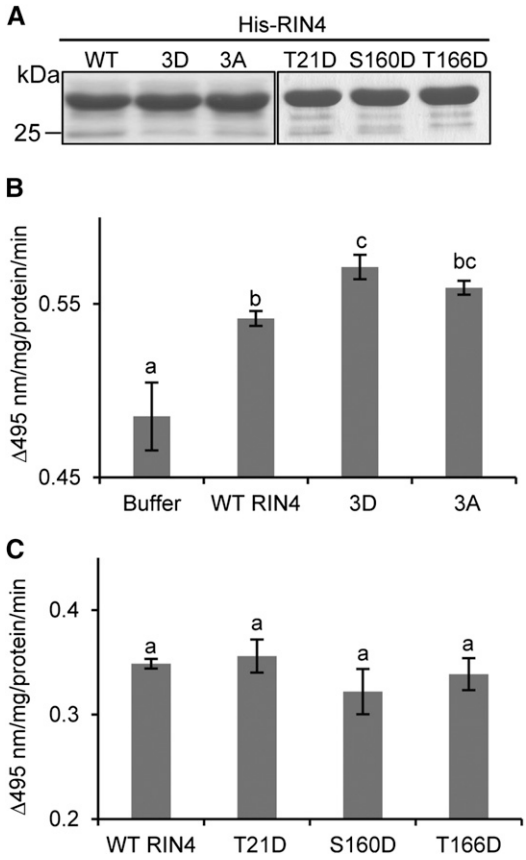

Figure 3. Purified Recombinant RIN4 Phosphorylation Mimics Enhance H^+-ATPase Activity.

Inside-out plasma membrane vesicles from the Arabidopsis *rpm1/rps2/rin4* mutant were incubated with different recombinant RIN4 proteins (RIN4 WT, 3D, 3A, T21D, S160D, or T166D) in the assay medium to measure H^+-ATPase activity. In this assay, the plasma membrane H^+-ATPase hydrolyzes ATP and pumps H^+ into vesicles, creating a pH gradient across the membrane. The pumping activity was measured by the pH probe acridine orange (Δ495 nm/mg protein/min).

(A) SDS-PAGE gel stained with Coomassie blue showing the purity of recombinant RIN4 wild type (WT), triple (3D), or single (T21D, S160D, and T166D) phosphorylation mimics and phosphorylation null (3A). Proteins were extracted at the same time but run on two separate SDS-PAGE gels.

(B) The RIN4 triple phosphorylation mimic (3D) enhances H^+-ATPase activity in vitro. Results represent means ± SD, $n = 3$. Different letters above bars indicate statistical differences in means, detected by a Fisher's LSD ($\alpha = 0.05$).

(C) RIN4 single phosphorylation mimics are unable to enhance H^+-ATPase activity in vitro. Results represent mean ± SD, $n = 3$. Statistical differences were detected as described in **(B)**. All assays used 50 μg of plasma membrane protein and 5 μg of recombinant RIN4.

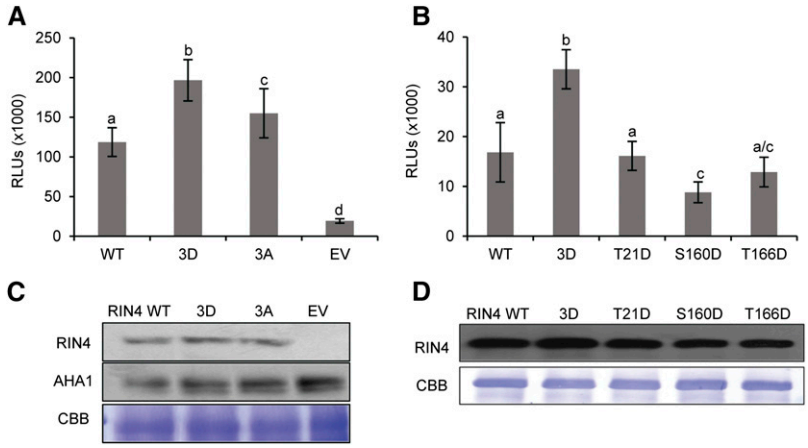

Figure 4. RIN4 Phosphorylation Mimics for All Three Residues Exhibit the Strongest Association with AHA1 in Planta.

AHA1 was coexpressed with different RIN4 phosphorylation mimics in *N. benthamiana* using *Agrobacterium tumefaciens*-mediated transient expression. The luciferase complementation assay used AHA1-NLuc and CLuc-RIN4 variants. Luciferin (1 mM) was infiltrated 48 h after Agrobacterium infiltration and the luminescence signal was quantified on a luminometer.

(A) The RIN4 phosphorylation mimic (RIN4 3D) exhibits the strongest enhanced association with AHA1 in *N. benthamiana.*

(B) The RIN4 triple (RIN4 3D) phosphorylation mimic, but not single phosphorylation mimics (RIN4 T21D, S160D, or T166D), show increased association with AHA1. For **(A)** and **(B)**, the bioluminescence signal in the leaf was captured using a CCD camera and the intensity was quantified by a luminometer. Results represent mean ± SD, $n \geq 5$. Different letters above bars indicate statistical differences in means, detected by a Fisher's LSD ($\alpha = 0.05$).

(C) Expression of CLuc-RIN4 and AHA1-NLuc in *N. benthamiana*. Anti-RIN4 and Anti-LUC antibody were used to detect RIN4 (top) and AHA1 (middle), respectively. An SDS-PAGE gel stained with Coomassie blue (CBB) was used to visualize protein loading (bottom).

(D) Anti-RIN4 protein gel blot confirmed RIN4 expression. The membrane was stained with Coomassie blue to visualize protein loading.

Although flg22 was able to induce stomatal closure in *ripk*, coronatine was unable to counter this effect (Supplemental Figure 5). Previously, we showed that virulent *Pto* DC3000 is unable to induce stomatal opening 3 h postinoculation in *rin4* KO lines (Liu et al., 2009b). Similarly, the *rpm1/rps2/rin4* genotype was able to rapidly close its stomata in response to flg22, but coronatine was unable to reopen its stomata (Supplemental Figure 5). Next, the ability of *Pto* DC3000 to induce stomatal reopening in *ripk* was examined using epidermal peels and light microscopy (Figure 5A). While *Pto* DC3000 was able to induce Col-0 stomatal opening 3 h posttreatment, stomata in the *ripk* KO remained closed (Figure 5A). These results demonstrate that *ripk* and *rin4* KO lines are insensitive to coronatine-induced stomatal reopening.

Pto DC3118 is a coronatine-deficient mutant of DC3000, carries a Tn5 insertion in *cfa6* (a gene essential for coronatine biosynthesis), and exhibits reduced virulence upon surface inoculation (Ma et al., 1991). Col-0 and *ripk* KO lines were spray inoculated with either *Pto* DC3000 or *Pto* DC3118 (Figure 5B). As previously reported, *ripk* lines exhibit enhanced disease resistance, and *Pto* DC3000 grew to 5-fold lower levels on this line after surface inoculation (Liu et al., 2011). *Pto* DC3118 grew to equal levels on Col-0 and *ripk* (Figure 5B). Taken together, these results indicate that the enhanced disease resistance phenotype observed in the *ripk* KO line primarily occurs at the level of pathogen entry.

Both *ripk* and *rin4* KOs exhibit similar stomatal phenotypes, indicating that RIN4 phosphorylation may play a role in coronatine-induced stomatal opening. However, we were unable to detect a major defect in coronatine-induced stomatal opening or flg22-induced closure in the complemented *T7-RIN4 3D* line 9-10 (Supplemental Figure 5A). For the confocal microscopy measurements, all data were combined for statistical analyses, making it difficult to detect differences in basal stomatal apertures between genotypes. Therefore, we decided to carefully analyze the basal stomatal apertures in complemented *T7-RIN4* lines using epidermal peels and light microscopy. We examined basal stomatal apertures of *rpm1/rps2*, wild-type RIN4, and phosphorylation RIN4 mimics at the same time. Stomata from wild-type *T7-RIN4* and *rpm1/rps2* did not exhibit a significant difference from one another with respect to their basal stomatal apertures (Figure 5C). The basal stomatal aperture for *T7-RIN4 3A* was not significantly wider than that of the *T7-RIN4* complemented line (Figure 5D). In contrast, the basal stomatal aperture for *T7-RIN4 3D* was significantly wider compared with *rpm1/rps2* (Figure 5C). This is consistent with the promotion of AHA activity after incubation with His6-RIN4 3D and a stronger interaction with AHA1 and RIN4 3D in planta (Figures 3 and 4). Although RIN4 3A exhibits enhanced association with AHA1, its ability to associate with and promote AHA activity is not as strong as RIN4 3D, potentially explaining the lack of a stomatal phenotype (Figures 3B and 4A). Next, *Pto* DC3118 was spray inoculated on *rpm1/rps2* and *T7-RIN4* complemented lines. Controls and wild-type *T7-RIN4* did not exhibit significant differences in *Pto* DC3118 bacterial growth 4 d postinoculation (Figure 5E). However, *T7-RIN4* 3D complemented lines exhibited significantly higher *Pto* DC3118 growth compared with *rpm1/rps2* 4 d after spray inoculation (Figure 5E). This is consistent with the wider basal stomatal apertures in *T7-RIN4* 3D, which could enable more bacteria to enter into the leaf interior and bypass the need for coronatine-induced stomatal opening.

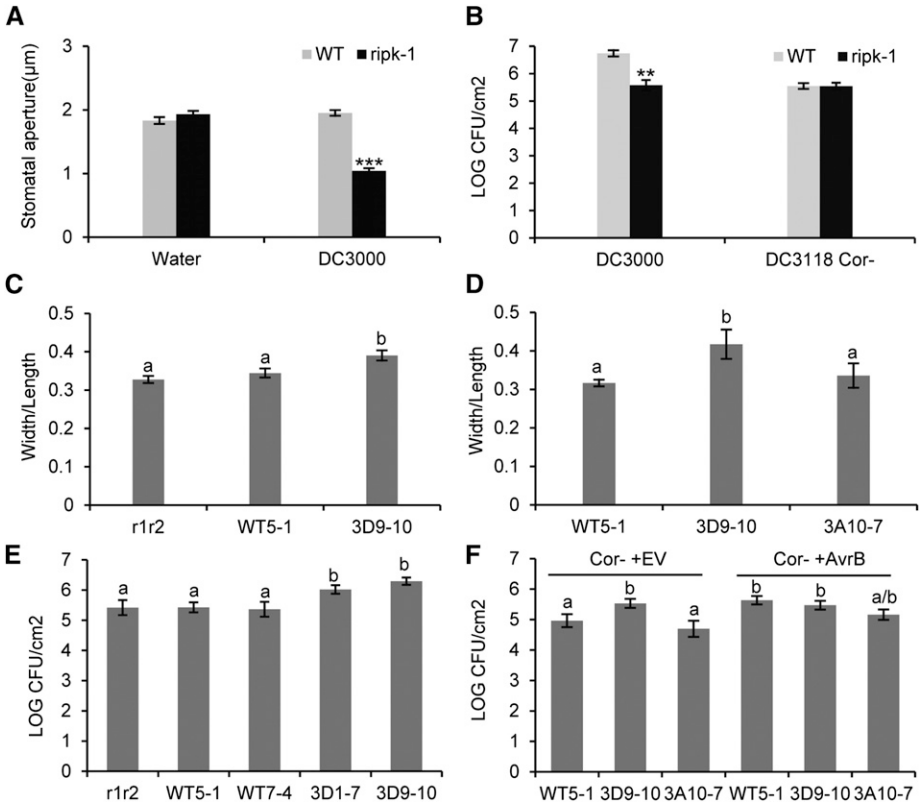

Figure 5. RIN4 Phosphorylation Mimics Display Wider Basal Stomatal Apertures, and the *ripk* Knockout Does Not Reopen Its Stomata in Response to Virulent *P. syringae*.

(A) The Arabidopsis *ripk* knockout line does not reopen stomata after treatment with virulent *Pto* DC3000. Stomatal apertures were measured in epidermal peels from wild-type Col-0 and the *ripk* knockout in the Col-0 background after incubation with either water or virulent *Pto* DC3000 at a concentration of 1×10^8 cfu/mL. Stomatal apertures were measured 3 h after treatment. Results represent means ± SE, $n = 30$. Statistical differences were detected by a two-tailed *t* test compared with the wild type; asterisks indicate $\alpha = 0.001$.

(B) The *ripk* knockout is more resistant after spray inoculation with *Pto* DC3000, but not the coronatine-deficient strain *Pto* DC3118. Four-week-old wild-type (WT) Col-0 or the *ripk* knockout (*ripk*-1) were spray-inoculated with 1×10^8 cfu/mL of *Pto* DC3000 or DC3118 Cor-. Bacterial population sizes were quantified 4 d postinoculation. Results represent mean ± SE, $n = 6$. Statistical differences were detected by a two-tailed *t* test compared with the wild type; asterisks indicate $\alpha = 0.01$.

(C) The RIN4 3D phosphorylation mimic exhibits wider basal stomatal apertures compared with controls. Basal stomatal apertures were measured 3 h after light treatment. Genotypes included *rpm1/rps2* (*r1r2*), *rpm1/rps2/rin4* complemented with *T7-RIN4* (WT), and *rpm1/rps2/rin4* complemented with *T7-RIN4 T21D/S160D/T166D* (3D). Results represent mean ± SE, $n \geq 100$. Different letters above bars indicate statistical differences in means, detected by a Fisher's LSD ($\alpha = 0.05$).

(D) The RIN4 3D phosphorylation mimic exhibits wider basal stomatal apertures compared with RIN4 phosphorylation null (3A). Basal stomata opening was measured in WT5-1, 3D 9-10, and 3A 10-7 lines. Results represent mean ± SE, $n \geq 90$. Statistical differences were detected as described in **(C)**.

(E) RIN4 phosphorylation mimic (3D) lines exhibit enhanced disease susceptibility to *Pto* DC3118 Cor-. Pathogen inoculation and bacterial population measurement were performed as described in **(B)**. Results represent means ± SE, $n = 6$. Statistical differences were detected as described in **(B)**.

(F) *Pto* DC3118 Cor- expressing AvrB exhibited enhanced bacterial growth in planta compared empty vector (EV) alone. RIN4 complementation lines were inoculated with *Pto* DC3118 Cor- expressing pBRR1-MCS5 (Cor- +EV) or *npro:AvrB:3xFlag* (Cor- +AvrB). Pathogen inoculation and bacterial growth measurement were performed as described in **(E)**. Results represent means ± SE, $n = 6$. Statistical differences were detected as described in **(C)**.

AvrB induces JA signaling and the expression of JA marker genes (He et al., 2004; Cui et al., 2010). Given RIN4's stomatal phenotype and the role of the JA mimic coronatine in inducing stomatal opening, we examined the ability of AvrB to promote growth of *Pto* DC3118 after spray inoculation. *Pto* DC3118 carrying AvrB-3xFLAG was able to enhance bacterial growth after spray inoculation compared with empty vector on the wild-type *T7-RIN4*, but was not able to enhance bacterial growth on *T7-RIN4 3D* (Figure 5F). The *T7-RIN4 3A* exhibited an intermediate phenotype (Figure 5F). Protein gel blotting with FLAG antisera verified AvrB expression in *Pto* DC3118 (Supplemental Figure 6).

Basal Phosphorylation of RIN4 Thr-166 Is Decreased upon flg22 Treatment

RIN4 not only plays an important role in NLR immune receptor activation, but it also acts to regulate basal plant defense against conserved MAMPs, such as bacterial flagellin (Kim et al.,

2005; Liu et al., 2009b; Chung et al., 2014). The hypothesis that phosphorylated RIN4 disrupts plant immune signaling to promote pathogen virulence in susceptible plant genotypes was examined. Wild-type RIN4 and RIN4 phosphorylation mimics were syringe infiltrated with the *Pto* ΔhrcC mutant, which is unable to deliver effectors and elicits strong PTI. Wild-type RIN4 complemented lines did not exhibit alterations in *Pto* ΔhrcC growth 4 d postinoculation, but *T7-RIN4 3D* exhibited enhanced bacterial growth (Figure 6A). We also examined a common PTI response, the extracellular ROS burst mediated by the NADPH oxidase RBOHD (Henry et al., 2013). Consistent with the *Pto* ΔhrcC growth curves, the flg22-induced ROS burst was not significantly different between controls and wild-type *T7-RIN4* complemented lines (Figure 6B; Supplemental Figure 7). In contrast, *T7-RIN4 3D* exhibited a significantly reduced ROS burst compared with controls after treatment with flg22 (Figures 6B and 6C; Supplemental Figure 7).

The Thr-21 and Thr-166 residues are conserved between RIN4 proteins present in land plants, but the Ser-160 residue is not (Afzal et al., 2013). Therefore, we focused on the role of Thr-21 and Thr-166 in suppressing PTI. In order to investigate the role of individual phosphorylated residues in RIN4-mediated PTI suppression, *rpm1/rps2/rin4* was complemented with *T7-RIN4 T21D, T7-RIN4 T166D* and *T7-RIN4 T21D/T166D* (Figure 6; Supplemental Figure 7). The *T7-RIN4 T166D* line exhibited significantly reduced ROS burst compared with controls after treatment with flg22 (Figure 6C; Supplemental Figure 7). *T7-RIN4 T21D* exhibited an intermediate reduction in ROS burst compared with the controls (Figure 6D; Supplemental Figure 7). The flg22-induced ROS burst in *T7-RIN4 T21D/T166D* was slightly lower than that of *T7-RIN4 T166D*, but again the difference was not statistically significant (Supplemental Figure 7C). Interestingly, the single T166D phosphomimetic line did not exhibit significantly more reduction in flg22-induced ROS compared with the 3D line. Thus, phosphorylation of Thr-166 is the most critical residue for suppressing PTI responses in the apoplast (Figure 6C; Supplemental Figure 7). These results are consistent with a recent study demonstrating that the RIN4 T166D phosphorylation mimic can suppress flg22-induced callose deposition, PTI-induced inhibition of virulent bacterial growth, and the flg22-induced ROS burst (Chung et al., 2014).

RIN4 Thr-166 phosphorylation is strongly induced in the presence of AvrB, but there is still a basal level of RIN4 Thr-166 phosphorylation in the absence of bacterial infection (Supplemental Figure 4). Visualization of basal pThr166 levels can be facilitated using a Femto maximum sensitivity enhanced chemiluminescent substrate to generate a signal for protein gel blotting. Therefore, we extracted protein from Col-0 10 min after infiltrating leaves with 1 μM flg22 peptide or water containing the surfactant Silwet L-77. Protein gel blotting with anti-phospho MAPK antibody verified activation of MAPK3/6 and PTI (Figure 7A). Proteins also were subjected to protein gel blot to probe for total levels of RIN4 as well as RIN4 pThr166. Comparison of RIN4 pThr166 levels after no treatment or infiltration with water demonstrated that water treatment does not grossly change basal pThr166 levels (Figure 7C). Interestingly, basal RIN4 pThr166 was decreased in the presence of flg22, indicating that RIN4 phosphorylation is downregulated after activation of PTI (Figures 7A and 7B).

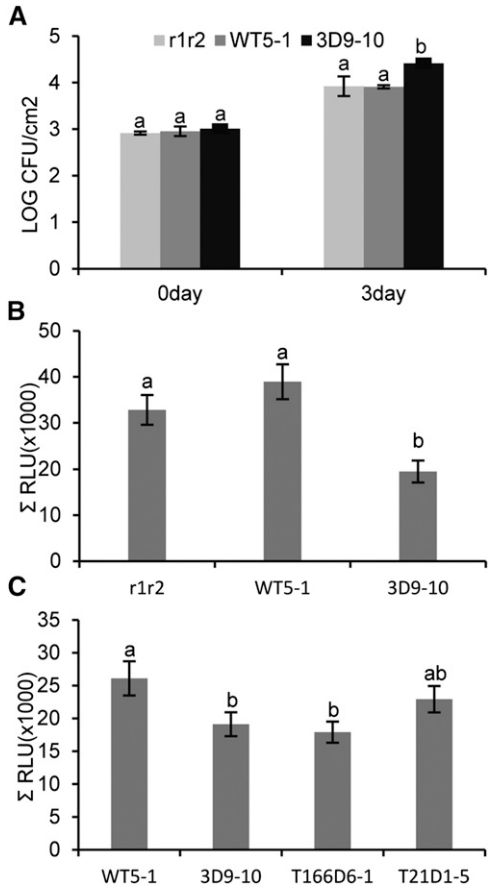

Figure 6. RIN4 Phosphorylation Mimics Exhibit Compromised PTI Responses.

(A) The RIN4 phosphorylation mimic (3D line 9-10) showed enhanced bacterial growth after inoculation with *Pto* DC3000 ΔhrcC. Genotypes included *rpm1/rps2* (*r1r2*), *rpm1/rps2/rin4* complemented with *T7-RIN4* (WT), and *rpm1/rps2/rin4* complemented with *T7-RIN4 T21D/S160D/T166D* (3D). Four-week-old Arabidopsis plants were syringe-inoculated with 1×10^5 cfu/mL of *Pto* DC3000 ΔhrcC and bacterial growth was quantified zero and 3 d postinoculation. Results represent means ± SE, $n = 6$.

(B) RIN4 phosphorylation mimics suppress the ROS burst upon flg22 perception. Leaf disks were harvested from *rpm1/rps2*, WT5-1, and 3D9-10, treated with 100nM flg22, and the ROS burst analyzed with a luminometer. Total ROS generation was monitored over 35 min. Results represent means ± SE, $n = 16$.

(C) RIN4 Thr-166 is the critical residue required for suppression of the flg22-induced ROS burst. ROS burst was measured in leaf discs of wild-type line 5-1, 3D line 9-10, T21D line 1-5, and T166D line 6-1 after 100 nM flg22 treatment as described in **(B)**. Total ROS generation was monitored over 35 min. Results represent means ± SE, $n = 16$. Different letters above bars indicate statistical differences in means, detected by a Fisher's LSD ($\alpha = 0.05$) for all panels.

AvrB can suppress flg22-induced PTI markers (Chung et al., 2014). Therefore, we analyzed the ability of flg22 perception to decrease pThr166 in the presence of AvrB expression. Transgenic lines expressing dexamethasone (Dex) inducible AvrB in the *rpm1-3* background were treated with 30 μM Dex followed by treatment with flg22 16 h after AvrB induction. The basal level

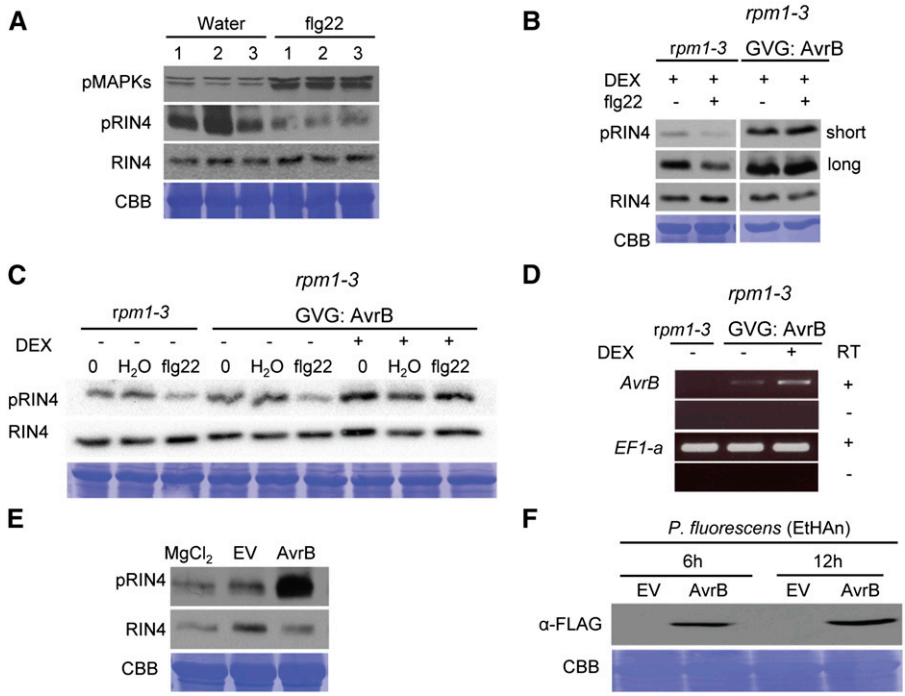

Figure 7. RIN4 Thr-166 Phosphorylation Is Suppressed during Flagellin Perception.

(A) The phosphorylation of RIN4 Thr-166 is decreased after flg22 treatment. Proteins were extracted 10 min after vacuum infiltration with 1 μM flg22 or water. Numbers indicate three biological repeats. RIN4 and RIN4 pThr166 (pRIN4) proteins were detected by anti-RIN4 and anti-pRIN4 Thr166 antibodies, respectively. In order to visualize basal RIN4 phosphorylation, a Femto enhanced chemiluminescence substrate was used to enable detection of a weak signal. Phosphorylated MAPK3/6 were detected by anti-p44/42 ERK antibody. The membrane was stained with Coomassie blue (CBB) to detect protein loading.

(B) Flg22 perception is unable to decrease pThr166 in the presence of strong ectopic AvrB expression. *rpm1-3* or *rpm1-3* carrying Dex-inducible *GVG:AvrB-HA* was treated with 30 μM Dex, then vacuum infiltrated with water or 1 μM flg22 and total proteins were extracted 10 min later. RIN4 and RIN4 pThr166 (pRIN4) proteins were detected by anti-RIN4 and anti-pRIN4 Thr-166 antibodies, respectively. Short and long indicate exposure time of the anti-pRIN4 blot. Protein samples were run on the same gel, but cropped to remove additional lanes. The membrane was stained with Coomassie blue to verify protein loading.

(C) Flg22 perception can decrease pThr166 in the presence of weak ectopic AvrB expression. Plant genotypes were treated with water or 3 μM Dex prior to infiltration with water or flg22 and immunoblotting as described in **(B)**.

(D) Detecting AvrB expression by RT-PCR. Four-week-old plants were not treated or treated with 3 μM Dex and total RNA was extracted for RT-PCR 16 h later. *ELONGATION FACTOR1-α* was used as a control for gene expression. RT, reverse transcriptase.

(E) *P. fluorescens* (EtHAn) expressing AvrB can induce RIN4 Thr-166 phosphorylation. *rpm1-3* plants were syringe-inoculated with 5×10^7 cfu/mL of *P. fluorescens* expressing a broad host range vector pBRR1 MCS5 (EV) or *npro:AvrB-3xFLAG*. $MgCl_2$ (10 mM) was used as the mock treatment. Total proteins were extracted 6 h postinfiltration. RIN4 and RIN4 pThr166 (pRIN4) proteins were detected by anti-RIN4 and anti-pRIN4 Thr-166 antibodies, respectively. The membrane was stained with Coomassie blue to verify protein loading.

(F) AvrB is expressed in the *rpm1-3* genotype after infection with *P. fluorescens* (EtHAn). Arabidopsis leaves were syringe-infiltrated as described in **(E)**. Total proteins were extracted from leaves at 6 and 12 h postinfiltration and AvrB was detected by immunoblotting using anti-FLAG antibody (top). The membrane stained with Coomassie blue verified protein loading (bottom).

of RIN4 pThr166 decreased in the *rpm1-3* background following flg22 treatment, but the basal level of RIN4 pThr166 remained elevated in the presence of strong ectopic AvrB expression even after treatment with flg22 (Figure 7B). In order to determine if this observation is dose dependent, we examined flg22-induced decrease of pThr166 during no and low (3 μM) Dex treatment (Figures 7C and 7D). AvrB expression was detectable at a low level in transgenic lines in the absence of Dex treatment (Figure 7D). We observed that flg22 perception was able to induce a decrease of pThr166 only in the absence of Dex treatment, indicating that this phenotype is AvrB dose dependent (Figure 7C).

Next, we examined RIN4 phosphorylation after delivery of AvrB from *Pseudomonas fluorescens* strain 0-1 using the Effector-to-Host Analyzer (EtHAn) system. The *P. fluorescens* EtHAn system has the *P. syringae* pv *syringae* type III secretion cluster integrated into its genome, enabling single effector delivery (Thomas et al., 2009). *P. fluorescens* EtHAn expressing either empty vector or AvrB-3XFLAG was infiltrated into *rpm1-3* leaves and the level of RIN4 as well as RIN4 pThr166 was examined 6 h postinfiltration. AvrB-3XFLAG expression was verified by protein gel blotting with antisera recognizing the FLAG epitope (Figure 7F). *rpm1-3* treated with $MgCl_2$ or *P. fluorescens*

expressing empty vector possessed low levels of RIN4 pThr166, while leaves treated with *P. fluorescens* expressing AvrB-3XFLAG exhibited high levels of RIN4 pThr166 (Figure 7E). These results indicate that type III delivered AvrB can effectively induce RIN4 pThr166 in the EtHAn system.

DISCUSSION

RIN4 is a fairly abundant plasma membrane-localized protein that is targeted by multiple pathogen effectors and guarded by the RPM1 and RPS2 immune receptors (Henry et al., 2013). Here, we focused on the role of effector-induced RIN4 phosphorylation in susceptible plant genotypes lacking the RPM1 and RPS2 immune receptors. There are 15 Arabidopsis proteins possessing homology to RIN4 and all share a common nitrate induced domain (NOI, Pfam: PF05627) (Afzal et al., 2013). The NOI domain is also present across land plants (Afzal et al., 2013). Importantly, NOI domains within RIN4 are targeted by AvrRpt2 for cleavage and AvrB to induce phosphorylation (Chisholm et al., 2005; Chung et al., 2011; Liu et al., 2011). Using CD spectroscopy, RIN4 was demonstrated to be primarily an intrinsically disordered protein whose flexibility is enhanced by phosphorylation (Figure 1) (Sun et al., 2014). Furthermore, Sun et al. (2014) demonstrated that RIN4, along with other NOI family members, exhibit intrinsic disorder, possessing molecular recognition features as well as ANCHOR-identified long binding regions, likely facilitating a transition to a more ordered structure upon protein complex formation. Intrinsic disorder has been shown to play an important role in the occurrence of some posttranslational modifications, including protein phosphorylation (Gao and Xu, 2012). Multiple phosphorylated RIN4 residues have been mapped in large-scale proteomic investigations, indicating that RIN4 is an important kinase target (Nühse et al., 2007). Given the shared NOI domain and intrinsic disorder among other NOI proteins, it is possible that their phosphorylation status is also altered in the presence of AvrB and AvrRpm1 for pathogen benefit.

Intrinsically disordered proteins frequently have multiple binding partners and can interact with proteins with high specificity and low affinity (Dyson and Wright, 2005). Therefore, we examined the effect of mimicking RIN4 phosphorylation on its association with a known binding partner, the plasma membrane H^+-ATPase (Liu et al., 2009b). RIN4 3D lines exhibit wider basal stomatal apertures, enhanced association with AHA1, and enhanced AHA enzymatic activity (Figures 3 and 4). Mimicking phosphorylation of all three residues was required for this phenotype. AHA activation leads to hyperpolarization of the guard cell membrane, activation of inward rectifying K^+ channels, and ultimately drives the uptake of solutes into guard cells, inducing stomatal opening (Elmore and Coaker, 2011). AHA1 and AHA2 constitutively active mutants or transgenic lines exhibit enhanced susceptibility to surface inoculation with *Pto* DC3000, have constitutively open stomata, and their stomata do not close in response to flg22 or other PTI elicitors (Merlot et al., 2007; Liu et al., 2009b). AHAs are regulated posttranslationally, particularly by phosphorylation of their C-terminal regulatory domain (Elmore and Coaker, 2011). Phosphorylated RIN4 could associate with a different set of client proteins, possibly bringing one or more kinases in proximity to AHA's C terminus, leading to pump activation (Liu et al., 2011). The *rin4* and *ripk* KOs are insensitive to coronatine-induced stomatal opening and exhibit reduced growth of *Pto* DC3118 after surface inoculation, indicating that RIN4 and specifically RIN4 phosphorylation is a critical component of the guard cell immune response (Liu et al., 2009b) (Figure 5).

Bacteria can use wounds or natural openings, such as stomata, to gain entry into the plant interior and cause disease. Not all *P. syringae* or other pathogenic bacterial strains possess coronatine, which mimics JA. Syringolin A, a nonribosomal peptide and polyketide synthase present in some *P. syringae* pv *syringae* strains, is able to counteract stomatal immunity (Schellenberg et al., 2010). Furthermore, some *P. syringe* effectors enhance growth on the surface of plant leaves (Lee et al., 2012). The *P. syringae* effector HopM1 can suppress stomatal immunity (Lozano-Durán et al., 2014). Recently, the AvrB, HopX1, and HopZ1a effectors have been demonstrated to activate JA signaling (Cui et al., 2010; Jiang et al., 2013; Gimenez-Ibanez et al., 2014). HopZ1a and HopX1 directly target JAZ proteins, which are transcriptional repressors of JA responsive genes (Jiang et al., 2013; Gimenez-Ibanez et al., 2014). AvrB activates JA signaling in a MAPK4-dependent manner (Cui et al., 2010). RIN4 can also interact with and is phosphorylated by MAPK4 (Cui et al., 2010). Type III delivered AvrB can also partially complement the *Pto* DC3118 coronatine mutant, resulting in enhanced bacterial growth upon spray inoculation (Figure 5).

RIN4 is present in significant quantities in guard cells as well as mesophyll cells and can regulate mesophyll-mediated PTI responses (Kim et al., 2005; Liu et al., 2009b). The basal level of RIN4 Thr-166 phosphorylation was strongly reduced after application of flg22, suggesting that FLS2 signaling suppresses phosphorylation of Thr-166 (Figure 7). In support of this, the *T7-RIN4 3D* and *T166D* phosphomimetic lines exhibited compromised PTI responses. These findings are also consistent with a recent study demonstrating that RIN4 T166D lines are compromised in PTI based responses (Chung et al., 2014). Chung et al. (2014) also found that RIN4 pThr166 is epistatic to pSer141. RIN4 pSer141 levels increase upon flg22 signaling, and mimicking Ser141 phosphorylation resulted in enhanced PTI responses (Chung et al., 2014). We examined the ability of flg22 perception to decrease pThr166 levels during AvrB expression (Figure 7). When strongly expressed in transgenic plants, AvrB is able to robustly induce phosphorylation of pThr166. In contrast, treatment with flg22 decreases levels of RIN4 pThr166 when little or no AvrB is present. However, flg22 treatment after strong AvrB expression did not decrease levels of RIN4 pThr166. Type III delivered AvrB from nonpathogenic *P. fluorescens*, which elicits robust PTI, is also able to induce phosphorylation of pThr166. These data are consistent with the notion that dose dependent delivery of AvrB is needed to inhibit flg22-mediated suppression of pThr166. During a natural infection, different cells could undergo a range of responses, with some cells perceiving MAMPs and undergoing PTI while other cells are subjected to effector-triggered susceptibility.

Previously, RIN4, RPM1, and RPS2 were demonstrated to associate with FLS2 by coimmunoprecipitation (Qi et al., 2011). RIPK is a member of the receptor-like cytoplasmic kinase

subfamily VIIa, whose family members also include BIK1. BIK1 is a critical regulator of PTI signaling, can phosphorylate FLS2 and RBOHD, facilitating the ROS burst induced by flg22 (Henry et al., 2013; Kadota et al., 2014; Li et al., 2014a). Given that the *ripk* KO is only partially compromised in RIN4 Thr-166 phosphorylation and activation of RPM1-mediated responses, it is possible that RIN4 is targeted by other kinases. Future experiments analyzing the association between RIN4 and other kinases will shed light onto how this important plant immune regulator affects PTI responses in the leaf interior.

METHODS

Purification of Recombinant RIN4, Secondary Structure Prediction, and Far-UV CD Spectroscopy

RIN4 intrinsic disorder was predicted by ProDOS, with a prediction false positive rate of 5% (Ishida and Kinoshita, 2007). *RIN4* cDNA was first PCR amplified and cloned into pDONR207 using Gateway technology (Invitrogen). PCR-based site directed mutagenesis was conducted to mutate RIN4 Thr-21, Ser-160, and Thr-166 residues to aspartic acid (D) or alanine (A) individually and in concert. The pETDUET-1 (Novagen) *Escherichia coli* expression vector was modified to be Gateway compatible for MCS1 and RIN4, and corresponding phosphorylation mimics were cloned into MCS1 as in frame fusions to the 6xHis tag using Gateway technology. RIN4 was expressed in *E. coli* and purified by Ni^{2+} affinity chromatography as described previously (Coaker et al., 2006).

For CD spectroscopy, RIN4 proteins were dialyzed for 16 h in 50 mM NaH_2PO_4, pH 8.0, and diluted to a concentration of 0.25 mg/mL. The protein concentration was quantified by Bradford assay and the purity was confirmed by an SDS-PAGE gel stained with Coomassie blue. CD spectra in the far-UV region (190 to 260 nm) were detected using a J-810 spectropolarimeter (Jasco) with a 0.1-mm path length cell. Each spectrum was scanned with a 1-nm bandwidth. Spectra were visualized with spectra manager software (Jasco). CD experiments were repeated twice using different batches of recombinant protein with similar results.

In Vitro Kinase Assay and Protein Partitioning under Native Conditions

Recombinant MBP-RIPK protein was purified as described previously and recombinant 6xHis RIN4 protein was purified as described above (Liu et al., 2011). In vitro assays were performed as described previously with slight modifications as described below (Liu et al., 2011). The kinase reaction was performed in kinase buffer (20 mM Tris-HCl, pH 7.5, 10 mM $MgCl_2$, 1 mM $CaCl_2$, 100 μM ATP, and 1 mM DTT). The protein ratio of RIPK:RIN4 was 2:1 (400 μg of RIPK and 200 μg of RIN4) in a total volume of 500 μL. Protein samples were incubated in kinase buffer for 30 min at 30°C. The kinase reaction in the absence of ATP was used as a negative control.

Following the kinase assay, RIPK protein was subsequently removed using an Amicon centrifugal filter unit (50 kD) based on molecular mass differences between MBP-RIPK (~95 kD) and 6xHis RIN4 (~28 kD). Protein samples were filtered through the Amicon unit at 14,000*g* for 15 min at 4°C. RIN4 and pRIN4 were subsequently subjected to CD spectroscopy following dialysis as described above. RIN4 purity was verified by SDS-PAGE electrophoresis. RIN4 phosphorylation was confirmed by immunoblotting using the anti-pRIN4 Thr-166 antibody at a concentration of 1:3000.

Gel Filtration Chromatography

6xHis-RIN4 (wild type, 3A, and 3D) proteins were induced as previously described (Coaker et al., 2006). Protein was purified on a 5-mL HisTrap HP column (GE Healthcare) coupled to an AKTA FPLC purification system. The column was washed with 50 column volumes of wash buffer containing 20 mM Tris-HCl, pH 8.0, 500 mM NaCl, and 40 mM imidazole. The protein was eluted with wash buffer supplemented with 250 mM imidazole. The proteins were concentrated to 0.7 mg/mL before applying to gel filtration chromatography (Superdex-200 10/300; GE Healthcare), which was equilibrated in buffer containing 20 mM Tris-HCl, pH 7.4, 200 mM NaCl, and 1 mM DTT. The flow rate was 0.5 mL/min, and the peak protein fractions were collected and visualized by SDS-PAGE coupled with Coomassie staining. All recombinant protein assays were repeated at least two times with independently purified batches of recombinant proteins. The gel filtration column was mapped using gel filtration markers for protein molecular mass (Sigma-Aldrich; MGWF 200).

Plant Materials and Growth Conditions

Arabidopsis thaliana seeds including Col-0, Landsberg *erecta*, individual knockout lines, and transgenic lines indicated in this study were stratified at 4°C for 2 d and sown in soil. Arabidopsis plants were grown in a controlled environmental chamber under the following conditions: 23°C, 70% relative humidity, a 10-h-light/14-h-dark photoperiod, and a light intensity of 85 μE/m^2/s. *Nicotiana benthamiana* plants were grown in the greenhouse under the following conditions: 25°C, 50% relative humidity, a 14-h-light/10-h-dark photoperiod, and a light intensity of 180 μE/m^2/s. The Arabidopsis *rps2/rpm1*, *rps2/rpm1/rin4*, *ripk* (in the Landsberg *erecta* background), and *ripk-1* (in the Col-0 background) genotypes were previously described (Mindrinos et al., 1994; Boyes et al., 1998; Mackey et al., 2002; Liu et al., 2011). In this article, *rps2* refers to the *rps2-101c* and *rpm1* refers to the *rpm1-3* mutation (Mindrinos et al., 1994; Boyes et al., 1998).

Transgenic Lines

To generate constructs for *RIN4* complementation, 2136 bp upstream from *RIN4*'s start codon were PCR amplified and cloned into pENTR/D-TOPO (Invitrogen). The N terminus of genomic *RIN4* (*gRIN4*) was fused to the T7 epitope tag by PCR and cloned behind the pENTR/D-TOPO native promoter *RIN4* construct using *Nco*I, resulting in *T7-RIN4*. PCR-based site directed mutagenesis was conducted to generate constructs for *RIN4* phosphorylation or dephosphorylation mimics. Thr-21, Ser-160, and Thr-166 residues were mutated to aspartic acid (D) to generate phosphorylation mimics (RIN4 T21D, T166D, T21D/T166D, or 3D) or mutated to alanine (A) to generate dephosphorylation mimics (RIN4 3A). *T7-RIN4* clones were recombined into the PGWb1 binary vector using Gateway technology (Nakagawa et al., 2007). The *rpm1/rps2/rin4* mutant was transformed with *npro:T7-gRIN4* constructs using the floral dip method and transformants selected on 50 μg/mL hygromycin (Bent, 2006). To determine RIN4 expression in transgenic Arabidopsis lines, total protein was extracted from 10-d-old seedlings using 2× Laemmli buffer (Laemmli, 1970). Total proteins were subjected to SDS-PAGE and protein gel blotting with affinity-purified rabbit polyclonal anti-RIN4 at a concentration of 1:3000. Secondary goat anti-rabbit IgG-HRP conjugate (Bio-Rad) was used at a concentration of 1:3000 for detection via enhanced chemiluminescence (Pierce). Individual T3 homozygous lines were used for all experiments.

Bacterial Strains and Disease Assays

Pto DC3000, the coronatine-deficient mutant *Pto* DC3118 Cor-, and the Type III secretion system deficient mutant *Pto* DC3000 ΔhrcC were grown on nutrient yeast-glycerol medium for 2 d at 28°C. *Pto* DC3000 expressing the *AvrB* effector or the pVSP61 empty vector alone was used to analyze RIN4 Thr-166 phosphorylation in *rpm1/rps2* 5 and 10 h after syringe infiltration with 5×10^7 colony-forming units (cfu)/mL of bacteria (Ashfield et al., 1995). To generate the coronatine-deficient mutant *Pto* DC3118 Cor- and *Pseudomonas fluorescens* (EtHAn) (Thomas et al., 2009) expressing the *AvrB* effector, the broad host rage vector pBRR1-MCS5

empty vector alone or *npro:AvrB:3xFLAG* were transferred into the respective strains by electroporation. AvrB effector expression was detected in Arabidopsis plants by immunoblotting using anti-FLAG antisera at a concentration of 1:1000. Antibiotics were used for bacterial selection at the following concentrations: 25 μg/mL kanamycin and 100 μg/mL rifampicin for *Pto* DC3000, *Pto* DC3118 Cor-, and *Pto* DC3000 ΔhrcC; 25 μg/mL kanamycin, 100 μg/mL rifampicin, and 10 μg/mL gentamycin for *Pto* DC3118 carrying pBRR1-MCS5; 50 μg/mL chloramphenicol, 50 μg/mL tetracyclin, and 50 μg/mL gentamycin for *P. fluorescens* (EtHAn) carrying pBRR1-MCS. For spray inoculation, 4-week-old Arabidopsis leaves were inoculated at a concentration of 1×10^8 cfu/mL bacteria. For syringe infiltration, 4-week-old Arabidopsis leaves were inoculated at a concentration of 1×10^5 cfu/mL bacteria. Spray and syringe inoculation as well as growth curves were conducted as previously described (Liu et al., 2009b). All experiments were repeated at least two times, with a minimum of six biological replicates per time point. Statistical differences were detected by Fisher's LSD following a significant F-statistic, $\alpha = 0.05$.

RIN4 Phosphorylation in Planta

Four-week-old Arabidopsis *rpm1/rps2* genotypes were syringe infiltrated with *Pto* DC3000 carrying the empty pVSP61 vector or pVSP61 expressing *AvrB* at a concentration of 10^8 cfu/mL to examine RIN4 phosphorylation induced by AvrB. Samples were harvested at 5 and 10 h postinfiltration and ground in protein extraction buffer (50 mM HEPES, pH 7.5, 50 mM NaCl, 10 mM EDTA, 0.2% Triton X-100, 1× complete protease inhibitors [Roche], and 1× Halt Phosphatase Inhibitor Cocktail [Thermo Scientific]). Protein concentrations were quantified using the 660-nm protein assay (Pierce) and equal amounts of protein per sample were subjected to SDS-PAGE, anti-RIN4 immunoblotting, and anti-pRIN4 immunoblotting as previously described (Liu et al., 2011). Four-week-old *rpm1* plants were syringe infiltrated with *P. fluorescens* (EtHAn) carrying the empty pBRR1 vector or pBRR1 expressing *npro:AvrB:3xFLAG* at a concentration of 5×10^7 cfu/mL to examine RIN4 phosphorylation induced by AvrB. Samples were harvested at 5 h postinfiltration. Protein samples were prepared and RIN4 phosphorylation was examined as described above.

To test basal RIN4 phosphorylation upon flg22 perception, total protein was extracted from 4-week-old Col-0 leaves 10 min after vacuum infiltration of 1 μm flg22 or water with 0.025% Silwett L-77. Samples were ground in protein extraction buffer and quantified as described above. The level of RIN4 phosphorylation was detected by anti-RIN4 and anti-pRIN4 immunoblotting as previously described (Liu et al., 2011). To detect activated MAPKs in response to flg22, pMAPK immunoblots were performed with anti-p42/44 ERK1/2 antibody (Cell Signaling; 4370S) at a concentration of 1:3000 in 5% BSA in TBST buffer (50 mM Tris, pH 7.6, 150 mM NaCl, and 0.05% Tween 20).

The *rpm1-3* genotype expressing *GVG:AvrB:HA* and *rpm1-3* was used to examine RIN4 pThr166 upon flg22 treatment (Nimchuk et al., 2000). Arabidopsis plants were not treated or sprayed with 3 or 30 μM Dex. At 16 h after Dex treatment, leaves were vacuum infiltrated with 1 μM flg22 or water and samples were harvested at 10 min after flg22 infiltration. A protein sample at time 0 (before spraying) was also taken. Protein sample preparation and anti-RIN4 immunoblotting were conducted as described above.

RT-PCR

RNA was extracted from 4-week-old *rpm1-3* or *rpm1-3* expressing GVG:AvrB-HA plants. Arabidopsis plants were either not treated or sprayed with 3 μM (Dex). The tissue was ground in liquid nitrogen and extracted in Trizol (Invitrogen). For RT-PCR, cDNA was synthesized using M-MLV reverse transcriptase (Promega) using 1 μg of total RNA from each sample. Primers pairs for *ELONGATION FACTOR 1-α* were used as an endogenous control and primers pairs for AvrB were used to detect the expression of AvrB (Supplemental Table 1). The experiment was repeated twice with three biological replicates per repetition.

Split-Luciferase Complementation Assay

RIN4 and *AHA1* cDNAs were PCR amplified and cloned into pENTR/D-TOPO (Invitrogen). RIN4 phosphorylation mimics and null were produced by PCR-based site directed mutagenesis as describe above. *RIN4* and *RIN4* phosphorylation mimics were cloned into the pCAMBIA CLuc, resulting in CLuc-RIN4 using Gateway technology (Chen et al., 2008). *AHA1* was cloned into the pCAMBIA NLuc vector using Gateway technology, resulting in AHA1-NLuc (Chen et al., 2008). Each construct was transformed into *Agrobacterium tumefaciens* strain GV3101. Agrobacterium suspensions containing respective *RIN4* variants and *AHA1* were coinfiltrated into *N. benthamiana* leaves at a final concentration of $OD_{600} = 0.4$ for each construct.

The split-luciferase complementation assay was performed as described previously, with minor modifications (Li et al., 2013). Two days after infiltration, 1 mM luciferin was infiltrated into the leaf, and the bioluminescence images were captured using the Kodak Image Station 4000R PRO (Carestream Molecular Imaging). To quantify bioluminescence using a luminometer, 1 mM luciferin was infiltrated into the leaf and plants were incubated for 10 min in the dark. Next, more than five leaf disks per construct were collected with a #2 hole punch and floated on water in a 96-well plate, and luminescence was quantified using a Tristar multimode reader (Berthold Technology). Total proteins were extracted from the leaf disks used for quantification of bioluminescence by grinding in Laemmli sample buffer (Laemmli, 1970). Statistical differences were detected by Fisher's LSD following a significant F-statistic, $\alpha = 0.05$. Protein concentrations were quantified using 660-nm protein assay (Pierce), and equal amounts of protein per sample were subjected to SDS-PAGE and anti-RIN4 immunoblotting as previously described (Liu et al., 2011). All experiments were repeated three times with similar results.

H^+-ATPase Activity Assay

For in vitro H^+-ATPase activity assays, individual recombinant RIN4 and RIN4 phosphorylation mimics were expressed and purified from *E. coli* as described above. Protein concentrations were determined by Bradford assay and their purity was analyzed by SDS-PAGE. Plasma membrane vesicles were purified from the *rpm1/rps2/rin4* genotype by an aqueous polymer two-phase system, and H^+-ATPase activity assays were measured by quenching of the ΔpH sensitive probe acridine orange as described previously (Liu et al., 2009b). Fifty micrograms of plasma membrane proteins were incubated with 5 μg of recombinant RIN4 protein to measure H^+-ATPase activity. Statistical differences were detected by Fisher's LSD following a significant F-statistic, $\alpha = 0.05$. Each experiment was repeated at least two times with independent plasma membrane and recombinant protein isolations.

Stomatal Aperture Measurements

In order to measure basal stomatal apertures, Arabidopsis *rps2/rpm1*, *npro:T7-gRIN4* wild type, *npro:T7-gRIN4* 3D, and *npro:T7-gRIN4* 3A lines were grown on soil in a controlled environmental chamber for 2.5 weeks as described above. The first and second true leaves were detached and floated on sterile water for 16 h and subsequently placed under white light for 3 h to induce to stomatal opening. In order to visualize stomatal apertures, epidermal peels were taken immediately before imaging. Medical adhesive (Hollister) was sprayed onto a microscope slide and the abaxial side of each leaf was placed in contact with the adhesive followed by gentle scraping with a razor blade to remove mesophyll cells. Stomatal images were taken by light microscopy (40× objective) coupled with a digital camera (Zeiss). Stomatal apertures were measured by calculating width-to-length ratios using Image J software (Liu et al., 2009b). A minimum of 90 individual apertures were measured per genotype. Measurement of stomatal apertures in the *ripk* knockout in response to *Pto* DC3000 was conducted as previously described (Liu et al., 2009b). Thirty individual stomata were measured per treatment. All experiments

were repeated at least three times with a minimum of three biological replicates for each experiment. Statistical differences were detected by Fisher's LSD following a significant F-statistic, $\alpha = 0.05$.

Flg22-induced stomatal closure and coronatine-induced stomatal reopening were imaged using confocal microscopy as previously described (Spallek et al., 2013). Cotyledons from 2-week-old seedlings were detached and immersed overnight in 500 μL of stomata opening buffer (SOB) (5 mM KCl, 50μM $CaCl_2$, and 10 mM MES-Tris, pH 6.15). For imaging, cotyledons were incubated in bright light for 2 h before treating with SOB (control), 10 μM flg22 in SOB, or 10 μM flg22 and 300 ng/mL coronatine in SOB for 2 h. Cotyledons were then mounted and placed in the bottom of a glass 96-well plate with 100 μL of water per well. Stomata were imaged using the Evotec *Opera* confocal laser scanning microscope (Perkin-Elmer), with a 405-nm laser and detection of 540/75 nm. Five fields and 25 z planes were taken per sample with 125 images taken per cotyledon. An average of 230 stomata were imaged per genotype, and image analyses was conducted on all data combined in R. Statistical differences were detected by Fisher's LSD following a significant F-statistic, $\alpha = 0.05$.

ROS Burst Assay

Leaf disks from 2- to 3-week-old Arabidopsis plants were sampled using a cork borer (4-mm diameter) and floated on sterile water for 16 h. The following day, the water was replaced with a solution of 17 mg/mL luminol (Sigma-Aldrich) and 10 mg/mL horseradish peroxidase (Sigma-Aldrich) containing 100 nM flg22. Luminescence was detected by the Tristar multimode reader (Berthold Technology). All experiments were repeated at least twice with a minimum of six biological replicates for each experiment.

Accession Numbers

All sequence data from this article can be found in the Arabidopsis Genome Initiative data library under the following accession numbers: *RIN4* (AT3G25070), *RIPK* (AT2G05940), *AHA1* (AT2G18960), *MAPK3* (AT3G45640), *MAPK6* (AT2G43790), and ELONGATION FACTOR1-α (AT5G60390).

Supplemental Data

Supplemental Figure 1. Thr-21 is the critical residue altering RIN4 secondary structure.

Supplemental Figure 2. Workflow for in vitro RIN4 phosphorylation and subsequent circular dichroism spectroscopy.

Supplemental Figure 3. Recombinant RIN4 and RIN4 phosphorylation mutants exhibit similar migration patterns by gel filtration chromatography.

Supplemental Figure 4. RIN4 phosphorylation is induced by AvrB in the *rpm1*/*rps2* mutant background.

Supplemental Figure 5. The *ripk* knockout is impaired in coronatine-induced stomatal reopening.

Supplemental Figure 6. AvrB is expressed in planta after infection with *Pseudomonas syringae* DC3118 Cor-.

Supplemental Figure 7. RIN4 phosphorylation mimics suppress ROS burst upon flg22 perception.

Supplemental Table 1. Primer sequences.

ACKNOWLEDGMENTS

We thank David Mackey for *rpm1*/*rps2*/*rin4* and *rpm1*/*rps2* seeds and Jeff Dangl for *GVG:AvrB-HA* seeds. We thank Jun Liu for his assistance in stomatal aperture measurements and Bryce Falk for the use of his ultracentrifuge. We thank Silvia Hilt and John Voss for guidance with CD spectroscopy. G.C. and D.H.L. were supported by National Institutes of Health Grant RO1GM092772 and the UC Davis Research Investment in Science and Engineering (RISE R1-091) awarded to G.C. S.R. and G.B. were supported by grants from the Gatsby Charitable Foundation and the European Research Council awarded to S.R.

AUTHOR CONTRIBUTIONS

D.H.L., G.B., and G.Y. performed the experiments. D.H.L. and G.C. wrote the article. D.H.L., G.C., and S.R. conceived the experiments.

Received September 18, 2014; revised June 22, 2015; accepted June 30, 2015; published July 21, 2015.

REFERENCES

Afzal, A.J., Kim, J.H., and Mackey, D. (2013). The role of NOI-domain containing proteins in plant immune signaling. BMC Genomics **14:** 327.

Ashfield, T., Keen, N.T., Buzzell, R.I., and Innes, R.W. (1995). Soybean resistance genes specific for different *Pseudomonas syringae* avirulence genes are allelic, or closely linked, at the RPG1 locus. Genetics **141:** 1597–1604.

Axtell, M.J., and Staskawicz, B.J. (2003). Initiation of RPS2-specified disease resistance in Arabidopsis is coupled to the AvrRpt2-directed elimination of RIN4. Cell **112:** 369–377.

Bent, A. (2006). *Arabidopsis thaliana* floral dip transformation method. Methods Mol. Biol. **343:** 87–103.

Bonardi, V., Tang, S., Stallmann, A., Roberts, M., Cherkis, K., and Dangl, J.L. (2011). Expanded functions for a family of plant intracellular immune receptors beyond specific recognition of pathogen effectors. Proc. Natl. Acad. Sci. USA **108:** 16463–16468.

Boyes, D.C., Nam, J., and Dangl, J.L. (1998). The *Arabidopsis thaliana* RPM1 disease resistance gene product is a peripheral plasma membrane protein that is degraded coincident with the hypersensitive response. Proc. Natl. Acad. Sci. USA **95:** 15849–15854.

Chen, H., Zou, Y., Shang, Y., Lin, H., Wang, Y., Cai, R., Tang, X., and Zhou, J.M. (2008). Firefly luciferase complementation imaging assay for protein-protein interactions in plants. Plant Physiol. **146:** 368–376.

Chisholm, S.T., Dahlbeck, D., Krishnamurthy, N., Day, B., Sjolander, K., and Staskawicz, B.J. (2005). Molecular characterization of proteolytic cleavage sites of the *Pseudomonas syringae* effector AvrRpt2. Proc. Natl. Acad. Sci. USA **102:** 2087–2092.

Chung, E.H., da Cunha, L., Wu, A.J., Gao, Z., Cherkis, K., Afzal, A.J., Mackey, D., and Dangl, J.L. (2011). Specific threonine phosphorylation of a host target by two unrelated type III effectors activates a host innate immune receptor in plants. Cell Host Microbe **9:** 125–136.

Chung, E.-H., El-Kasmi, F., He, Y., Loehr, A., and Dangl, J.L. (2014). A plant phosphoswitch platform repeatedly targeted by type III effector proteins regulates the output of both tiers of plant immune receptors. Cell Host Microbe **16:** 484–494.

Coaker, G., Zhu, G., Ding, Z., Van Doren, S.R., and Staskawicz, B. (2006). Eukaryotic cyclophilin as a molecular switch for effector activation. Mol. Microbiol. **61:** 1485–1496.

Cui, H., Wang, Y., Xue, L., Chu, J., Yan, C., Fu, J., Chen, M., Innes, R.W., and Zhou, J.M. (2010). Pseudomonas syringae effector

protein AvrB perturbs Arabidopsis hormone signaling by activating MAP kinase 4. Cell Host Microbe **7:** 164–175.

Dyson, H.J., and Wright, P.E. (2005). Intrinsically unstructured proteins and their functions. Nat. Rev. Mol. Cell Biol. **6:** 197–208.

Elmore, J.M., and Coaker, G. (2011). The role of the plasma membrane H^+-ATPase in plant-microbe interactions. Mol. Plant **4:** 416–427.

Gao, J., and Xu, D. (2012). Correlation between posttranslational modification and intrinsic disorder in protein. Pac. Symp. Biocomput. **2012:** 94–103.

Gao, Z., Chung, E.H., Eitas, T.K., and Dangl, J.L. (2011). Plant intracellular innate immune receptor Resistance to *Pseudomonas syringae* pv. *maculicola* 1 (RPM1) is activated at, and functions on, the plasma membrane. Proc. Natl. Acad. Sci. USA **108:** 7619–7624.

Gimenez-Ibanez, S., Boter, M., Fernández-Barbero, G., Chini, A., Rathjen, J.P., and Solano, R. (2014). The bacterial effector HopX1 targets JAZ transcriptional repressors to activate jasmonate signaling and promote infection in Arabidopsis. PLoS Biol. **12:** e1001792.

Greenfield, N.J. (2006). Using circular dichroism spectra to estimate protein secondary structure. Nat. Protoc. **1:** 2876–2890.

He, P., Chintamanani, S., Chen, Z., Zhu, L., Kunkel, B.N., Alfano, J.R., Tang, X., and Zhou, J.M. (2004). Activation of a COI1-dependent pathway in Arabidopsis by *Pseudomonas syringae* type III effectors and coronatine. Plant J. **37:** 589–602.

Henry, E., Yadeta, K.A., and Coaker, G. (2013). Recognition of bacterial plant pathogens: local, systemic and transgenerational immunity. New Phytol. **199:** 908–915.

Ishida, T., and Kinoshita, K. (2007). PrDOS: prediction of disordered protein regions from amino acid sequence. Nucleic Acids Res. **35:** W460–W464.

Jeuken, M.J., Zhang, N.W., McHale, L.K., Pelgrom, K., den Boer, E., Lindhout, P., Michelmore, R.W., Visser, R.G., and Niks, R.E. (2009). Rin4 causes hybrid necrosis and race-specific resistance in an interspecific lettuce hybrid. Plant Cell **21:** 3368–3378.

Jiang, S., Yao, J., Ma, K.W., Zhou, H., Song, J., He, S.Y., and Ma, W. (2013). Bacterial effector activates jasmonate signaling by directly targeting JAZ transcriptional repressors. PLoS Pathog. **9:** e1003715.

Kadota, Y., Sklenar, J., Derbyshire, P., Stransfeld, L., Asai, S., Ntoukakis, V., Jones, J.D., Shirasu, K., Menke, F., Jones, A., and Zipfel, C. (2014). Direct regulation of the NADPH oxidase RBOHD by the PRR-associated kinase BIK1 during plant immunity. Mol. Cell **54:** 43–55.

Kim, M.G., da Cunha, L., McFall, A.J., Belkhadir, Y., DebRoy, S., Dangl, J.L., and Mackey, D. (2005). Two *Pseudomonas syringae* type III effectors inhibit RIN4-regulated basal defense in Arabidopsis. Cell **121:** 749–759.

Laemmli, U.K. (1970). Cleavage of structural proteins during the assembly of the head of bacteriophage T4. Nature **227:** 680–685.

Lee, J., Teitzel, G.M., Munkvold, K., del Pozo, O., Martin, G.B., Michelmore, R.W., and Greenberg, J.T. (2012). Type III secretion and effectors shape the survival and growth pattern of *Pseudomonas syringae* on leaf surfaces. Plant Physiol. **158:** 1803–1818.

Li, L., Li, M., Yu, L., Zhou, Z., Liang, X., Liu, Z., Cai, G., Gao, L., Zhang, X., Wang, Y., Chen, S., and Zhou, J.M. (2014a). The FLS2-associated kinase BIK1 directly phosphorylates the NADPH oxidase RbohD to control plant immunity. Cell Host Microbe **15:** 329–338.

Li, M., et al. (2014b). Proline isomerization of the immune receptor-interacting protein RIN4 by a cyclophilin inhibits effector-triggered immunity in Arabidopsis. Cell Host Microbe **16:** 473–483.

Li, W., Yadeta, K.A., Elmore, J.M., and Coaker, G. (2013). The *Pseudomonas syringae* effector HopQ1 promotes bacterial virulence and interacts with tomato 14-3-3 proteins in a phosphorylation-dependent manner. Plant Physiol. **161:** 2062–2074.

Lindeberg, M., Cunnac, S., and Collmer, A. (2012). *Pseudomonas syringae* type III effector repertoires: last words in endless arguments. Trends Microbiol. **20:** 199–208.

Liu, J., Elmore, J.M., and Coaker, G. (2009a). Investigating the functions of the RIN4 protein complex during plant innate immune responses. Plant Signal. Behav. **4:** 1107–1110.

Liu, J., Elmore, J.M., Lin, Z.J., and Coaker, G. (2011). A receptor-like cytoplasmic kinase phosphorylates the host target RIN4, leading to the activation of a plant innate immune receptor. Cell Host Microbe **9:** 137–146.

Liu, J., Elmore, J.M., Fuglsang, A.T., Palmgren, M.G., Staskawicz, B.J., and Coaker, G. (2009b). RIN4 functions with plasma membrane H^+-ATPases to regulate stomatal apertures during pathogen attack. PLoS Biol. **7:** e1000139.

Lozano-Durán, R., Bourdais, G., He, S.Y., and Robatzek, S. (2014). The bacterial effector HopM1 suppresses PAMP-triggered oxidative burst and stomatal immunity. New Phytol. **202:** 259–269.

Luo, Y., Caldwell, K.S., Wroblewski, T., Wright, M.E., and Michelmore, R.W. (2009). Proteolysis of a negative regulator of innate immunity is dependent on resistance genes in tomato and *Nicotiana benthamiana* and induced by multiple bacterial effectors. Plant Cell **21:** 2458–2472.

Ma, S.W., Morris, V.L., and Cuppels, D.A. (1991). Characterization of a DNA region required for production of the phytotoxin coronatine by *Pseudomonas syringae* pv. tomato. Mol. Plant Microbe Interact. **4:** 69–74.

Mackey, D., Belkhadir, Y., Alonso, J.M., Ecker, J.R., and Dangl, J.L. (2003). Arabidopsis RIN4 is a target of the type III virulence effector AvrRpt2 and modulates RPS2-mediated resistance. Cell **112:** 379–389.

Mackey, D., Holt III, B.F., Wiig, A., and Dangl, J.L. (2002). RIN4 interacts with *Pseudomonas syringae* type III effector molecules and is required for RPM1-mediated resistance in Arabidopsis. Cell **108:** 743–754.

McDowell, J.M., and Simon, S.A. (2006). Recent insights into R gene evolution. Mol. Plant Pathol. **7:** 437–448.

Melotto, M., Underwood, W., Koczan, J., Nomura, K., and He, S.Y. (2006). Plant stomata function in innate immunity against bacterial invasion. Cell **126:** 969–980.

Merlot, S., Leonhardt, N., Fenzi, F., Valon, C., Costa, M., Piette, L., Vavasseur, A., Genty, B., Boivin, K., Müller, A., Giraudat, J., and Leung, J. (2007). Constitutive activation of a plasma membrane H^+-ATPase prevents abscisic acid-mediated stomatal closure. EMBO J. **26:** 3216–3226.

Meyers, B.C., Kozik, A., Griego, A., Kuang, H., and Michelmore, R.W. (2003). Genome-wide analysis of NBS-LRR-encoding genes in Arabidopsis. Plant Cell **15:** 809–834.

Mindrinos, M., Katagiri, F., Yu, G.L., and Ausubel, F.M. (1994). The *A. thaliana* disease resistance gene RPS2 encodes a protein containing a nucleotide-binding site and leucine-rich repeats. Cell **78:** 1089–1099.

Mukhtar, M.S., et al.; European Union Effectoromics Consortium (2011) Independently evolved virulence effectors converge onto hubs in a plant immune system network. Science **333:** 596–601.

Nakagawa, T., Kurose, T., Hino, T., Tanaka, K., Kawamukai, M., Niwa, Y., Toyooka, K., Matsuoka, K., Jinbo, T., and Kimura, T. (2007). Development of series of gateway binary vectors, pGWBs, for realizing efficient construction of fusion genes for plant transformation. J. Biosci. Bioeng. **104:** 34–41.

Narusaka, M., Shirasu, K., Noutoshi, Y., Kubo, Y., Shiraishi, T., Iwabuchi, M., and Narusaka, Y. (2009). RRS1 and RPS4 provide

a dual Resistance-gene system against fungal and bacterial pathogens. Plant J. **60:** 218–226.

Nimchuk, Z., Marois, E., Kjemtrup, S., Leister, R.T., Katagiri, F., and Dangl, J.L. (2000). Eukaryotic fatty acylation drives plasma membrane targeting and enhances function of several type III effector proteins from *Pseudomonas syringae*. Cell **101:** 353–363.

Nühse, T.S., Bottrill, A.R., Jones, A.M., and Peck, S.C. (2007). Quantitative phosphoproteomic analysis of plasma membrane proteins reveals regulatory mechanisms of plant innate immune responses. Plant J. **51:** 931–940.

Qi, Y., Tsuda, K., Glazebrook, J., and Katagiri, F. (2011). Physical association of pattern-triggered immunity (PTI) and effector-triggered immunity (ETI) immune receptors in Arabidopsis. Mol. Plant Pathol. **12:** 702–708.

Schellenberg, B., Ramel, C., and Dudler, R. (2010). *Pseudomonas syringae* virulence factor syringolin A counteracts stomatal immunity by proteasome inhibition. Mol. Plant Microbe Interact. **23:** 1287–1293.

Selote, D., and Kachroo, A. (2010). RPG1-B-derived resistance to AvrB-expressing *Pseudomonas syringae* requires RIN4-like proteins in soybean. Plant Physiol. **153:** 1199–1211.

Slootweg, E., et al. (2010). Nucleocytoplasmic distribution is required for activation of resistance by the potato NB-LRR receptor Rx1 and is balanced by its functional domains. Plant Cell **22:** 4195–4215.

Spallek, T., Beck, M., Ben Khaled, S., Salomon, S., Bourdais, G., Schellmann, S., and Robatzek, S. (2013). ESCRT-I mediates FLS2 endosomal sorting and plant immunity. PLoS Genet. **9:** e1004035.

Spoel, S.H., and Dong, X. (2012). How do plants achieve immunity? Defence without specialized immune cells. Nat. Rev. Immunol. **12:** 89–100.

Sun, X., Greenwood, D.R., Templeton, M.D., Libich, D.S., McGhie, T.K., Xue, B., Yoon, M., Cui, W., Kirk, C.A., Jones, W.T., Uversky, V.N., and Rikkerink, E.H.A. (2014). The intrinsically disordered structural platform of the plant defence hub protein RPM1-interacting protein 4 provides insights into its mode of action in the host-pathogen interface and evolution of the nitrate-induced domain protein family. FEBS J. **281:** 3955–3979.

Tamaki, S., Dahlbeck, D., Staskawicz, B., and Keen, N.T. (1988). Characterization and expression of two avirulence genes cloned from *Pseudomonas syringae* pv. *glycinea*. J. Bacteriol. **170:** 4846–4854.

Thomas, W.J., Thireault, C.A., Kimbrel, J.A., and Chang, J.H. (2009). Recombineering and stable integration of the *Pseudomonas syringae* pv. *syringae* 61 hrp/hrc cluster into the genome of the soil bacterium *Pseudomonas fluorescens* Pf0-1. Plant J. **60:** 919–928.

Ueno, K., Kinoshita, T., Inoue, S., Emi, T., and Shimazaki, K. (2005). Biochemical characterization of plasma membrane H+-ATPase activation in guard cell protoplasts of *Arabidopsis thaliana* in response to blue light. Plant Cell Physiol. **46:** 955–963.

Wilton, M., Subramaniam, R., Elmore, J., Felsensteiner, C., Coaker, G., and Desveaux, D. (2010). The type III effector HopF2Pto targets Arabidopsis RIN4 protein to promote *Pseudomonas syringae* virulence. Proc. Natl. Acad. Sci. USA **107:** 2349–2354.

Xin, X.F., and He, S.Y. (2013). *Pseudomonas syringae* pv. *tomato* DC3000: a model pathogen for probing disease susceptibility and hormone signaling in plants. Annu. Rev. Phytopathol. **51:** 473–498.